DD

LAPP-EXP-94.06
March 1994

sw 9419

A FIRST ELECTROMAGNETIC CALORIMETER PROTOTYPE OF $PbWO_4$ CRYSTALS

O.V. Buyanov[1], R. Chipaux[2], A.A. Fyodorov[3], V.A. Kachanov[1], V.Yu. Khodyrev[1], M.V. Korzhik[4], J.L. Faure[2], J.P. Peigneux[5], M. Poulet[5], Yu.D. Prokoshkin[1], P. Rebourgeard[2], V.V. Rykalin[1], P. Shagin[1], P.A. Semenov[1], A.V. Singovsky[1] and V.L. Solovianov[1].

ABSTRACT

The main properties of $PbWO_4$ crystals have been measured. They are of particular interest for electromagnetic calorimetry. Beam tests of 21-cells matrix prototype are reported. An energy resolution better than 1% has been achieved for electrons energies larger than 25 GeV.

(Submitted to Nucl. Instr. and Methods)

1) Institute for High Energy Physics, Protvino, Russia.
2) DAPNIA, CEA Saclay, France.
3) Radiation Instruments and New Components Ltd., Minsk, Belarus.
4) Institute of Nuclear Problems, Minsk, Belarus.
5) LAPP/IN2P3, Annecy, France.

1. INTRODUCTION

The lead tungstate scintillating crystal $PbWO_4$ [1-6] (hereafter designated as PWO) has recently been shown to be amongst the most promising candidates for future electromagnetic (EM) calorimetry, together with CeF_3 [7] and PbF_2, a Cherenkov light radiator [8]. CeF_3 provides a high light yield and PbF_2 has fast timing properties with a high stopping power. But PWO crystals present a whole set of physical and chemical parameters (Table 1) which are attractive for large EM calorimeters in the extreme conditions that are foreseen for example at LHC. Despite a moderate mechanical hardness (Moh = 4), it is easy to machine and polish. PWO is grown from a mixture of PbO and WO_3 oxides by the Czochralski method at a rather moderate temperature. The recent study of the light emission mechanism of PWO samples grown in various conditions allows to control the growing technology in order to optimise desirable characteristics [9-10].

This work presents the first beam tests of electromagnetic calorimeter prototypes made of large size crystals ($\geq 20\ X_0$) at IHEP Protvino, with 4 cells grown in different conditions, and at CERN, with a matrix of 21 cells grown in optimised conditions as much as possible.

2. SCINTILLATION AND OPTICAL PROPERTIES OF PWO CRYSTAL

The PWO crystals are grown in platinum crucibles in an atmosphere similar to air in composition. A reference sample (1 x 1 x 1 cm^3) and a long bar have been cut out from a series of ingots (~ 240 mm long, Ø ~ 32 mm).

The luminescence characteristics of a reference crystal are presented in Fig. 1. A large energy gap separates the maximum of luminescence emission around 480 nm and the strong absorption edge below 350 nm. The scintillation light is a superposition of several bands between λ = 420 nm and 650 nm [9]. Crystals have been grown in conditions that favour green luminescence.

The scintillation kinetics (or decay time) of PWO was measured by the start-stop method with a ^{22}Na source and a Lecroy 3001 QVT analyser. Measurements shown in Fig. 2 have been fitted by a sum of 3 exponential functions and a constant background. Decay times are $\tau_1 = (2 \pm 0.1)$ns, $\tau_2 = (7.4 \pm 0.3)$ns and $\tau_3 = (26 \pm 3)$ns respectively. Their relative intensities

are 41%, 39% and 20% after background subtraction. In Fig. 3a, the observed scintillation yield for PWO and BGO samples of the same dimensions (20 x 20 x 40 mm^3) wrapped in millipore (a diffusing material) are shown for different radioactive excitation sources. The light was detected by a photomultiplier tube (PM) Philips XP2262 coupled to the crystal with the Dow Corning Q_2-3067 optical compound (refractive index n = 1.48). All spectra have been measured with a Lecroy QVT pulse charge analyser. The gate widths were 350 ns for BGO and 35 ns for PWO, respectively. In the case of BGO irradiated by ^{137}Cs, the signal was attenuated by 24 db. The mean value of the pedestals corresponds to the same channel number, in both Fig. 3a and 3b.

The measured scintillation efficiency of PWO is 5% of that of BGO when the resolution of the ^{137}Cs photopeak (0.660 MeV) is used to estimate the number of photoelectrons. Fig. 3a also shows the 60 keV photopeak obtained with BGO and ^{241}Am source. Fig. 3b represents the ^{137}Cs γ-peak and the 4.4 MeV Am-Be source γ-peak detected by a (2.2 x 2.2 x 2.4 cm^3) PWO crystal. Here high voltage settings allow a direct comparison of spectra without attenuation. The ratios of photopeak positions and of energies are in agreement.

3. RADIATION HARDNESS

The γ-radiation hardness of PWO is related to charge exchange processes in Pb^{3+} defect centers [10]. It has been checked with a 500 R/s intensity ^{60}Co source at room temperature (300°K). Crystals with a large number of Pb^{3+} centers are initially slightly yellowish. Their transparency increases under small irradiation doses and decreases above a 10^5 rad absorbed dose, but it recovers very fast. Fig. 4a shows such a recovery after 10 days without any special UV or visible light treatment.

Negligible changes (Fig. 4b) of transparency are observed up to 5 Mrad in a more transparent crystal grown with less Pb^{3+} centers. Further production of crystals for the calorimeter prototype has been made along this line.

A sample (2 x 2 x 2.4 cm^3) has been irradiated with neutrons from the Saclay reactor ULYSSE. Experimental conditions of irradiation are described elsewhere [11]. Fast neutrons cumulative fluxes range from 10^{12} to 10^{14} n/cm^2. The γ contamination amounts to 1.2 Mrad

for 10^{14} fast n/cm^2. Accompanying thermal and epithermal neutron fluxes are three times larger than the fast neutron flux. Due to activation, the transmission has been measured after a delay from 1 to 2 weeks according to the initial dose, meanwhile samples were kept in darkness to prevent any annealing effect.

The irradiation effect on light attenuation is shown in Fig. 4c. The corresponding absorption coefficient variation Δk (defined by $T_{irrad}/T_{init} = e^{-\Delta KL}$) is displayed in Fig. 4d. Almost no influence is observed up to 10^{13} n/cm^2. The variation becomes significant above this fluence but remains very low. After 10^{14} n/cm^2 the radiation induced attenuation length is about 1 m.

4. BEAM TESTS

4.1 Tests Conditions

a) at IHEP Protvino in an electron beam from 4 to 26 GeV/c (Spring 93) with a momentum spread $\sigma p/p \sim 2\%$ [12] :

Four PWO crystals grown in different conditions have been studied. Their cross-section was 22 x 22 mm^2 with lengths ranging from 150 to 180 mm (17-20 X_0). They were assembled inside a 4 x 4 matrix, as shown in Fig. 5, where they occupy positions PWO1, PWO2, PWO5, PWO6. The others cells were made of Cherenkov radiators like $Gd_3 Ga_5 O_{12}$ alias (GGG) or $NaBi(WO_4)_2$ alias (NBW) with close refractive index and radiation length (Table 1). The photomultipliers were Philips XP1911 or FEU-147. The crystals were polished and wrapped in aluminised mylar. The scintillation yield of each cell had been previously measured with a Philips XP2020Q and with a multialcali photocathode FEU-84. These PMs have a photocathode larger than the crystal output area. The light collection geometrical factor is $\varepsilon_g = 1$. Optical coupling was done with DowCorning Q2-3067.

b) at CERN in an electron beam of 10, 25 and 100 GeV/c available in the H8 beam of the SPS North Area (Autumn 93), with a momentum spread $\sigma p/p \sim 0.4\%$ [9] :

A matrix detector of 21 crystals has been assembled. A Philips XP1911 phototube was attached to each crystal. The matrix cells were separated by 50 μm of iron sheets. They

were wrapped in reflecting millipore foils and protected by mylar. There was thus a total of 0.35 mm of material between the cells. After considering the results of the first tests at IHEP, the lateral dimensions of the cells have been chosen to be 20 x 20 mm^2. Their length was at least 20 X_0. The photocathode partially covered the output area of the crystals with a light collection geometrical factor $\varepsilon_g = 0.38$. Fig. 6 displays the matrix structure. Signals were digitised by the 12 bit ADC data acquisition system of GAMS NA12.

4.2 Single Cell Tests

At IHEP, the spectra produced by 26 GeV/c electrons in GGG and in PWO associated to the same XP2020Q PM have been compared. The $\sigma A/A$ resolution of the PWC peak is ~ 1%, twice better than that of a Cherenkov GGG cell. Taking the mean quantum efficiency for Cherenkov light (~ 20%) and for PWO scintillation light (~ 7%) into account, a factor 10 between Cherenkov and PWO scintillation light intensity can be evaluated in agreement with the previous observation [13].

The collected charge as a function of the gate width for various PWO and GGG cells have been measured after 95 m of 50Ω cable. Results for the four PWO cells and one GGG cell are shown in Fig. 7a, taking as a reference the charge amplitude obtained with a 400 ns gate. PWO6 is almost as fast as the Cherenkov radiator GGG. It has been selected as a reference for further crystal production. The pulse width (recorded with a XP2020Q PM) is 15 ns (FWHM) and 25 ns (at 10% of the maximum amplitude).

At CERN, 100 GeV/c electron signals measured with a XP1911 PM are shown in Fig. 7b. They were observed with a Tektronix 2467B oscilloscope after a 4 m long 50 Ω cable (30 ns separate the two vertical bars). The rise time is ~ 5 ns. 85% of the signal lies inside a ~ 35 ns window.

4.3 Coordinate Resolution and Shower Profile Measurements

The matrix structure shown in Fig. 5 has also been used to determine the profile of the shower of 26 GeV electrons (IHEP). The beam was scanned across the PWO6 and PWO5

cells, as indicated by the arrow. Fig. 8a displays the horizontal position of the center of gravity of the calibrated pulse amplitudes in each matrix cell as a function of the impact of the incident electron as determined with a 200 μm pitch silicon microstrip detector. The origin of the coordinates was just at the interface between PWO5 and PWO6. After applying a correction procedure described in [14] real impact coordinates were obtained. The position resolution σ_x of the center of gravity, that is displayed in Fig. 8b with the origin at the center of the cell, is less than 400 μm near the edge and it rises to 900 μm in the center.

The measured 26 GeV electron shower profile is shown in Fig. 9a as the fraction A_6/A_{tot} of the charge amplitude that is collected in PWO6 as a function of beam position. The origin is the center of PWO6. Up to 86% of the electromagnetic shower energy is absorbed in the central 22 x 22 mm^2 cell. For comparison, Fig. 9b displays the shower profiles for GGG (1), NBW (2), PWO (3) and TF1(SF2) (4) lead glass. The profile is twice narrower in heavy crystals than in TF1.

4.4 Muon Beam Tests and Attenuation Length

The attenuation length of the scintillation light through PWO has been measured with muons crossing cells perpendicularly to their axis. Fig. 10a displays scans of three crystals (20 X_0, CERN matrix) as a function of the distance of the muon impact to the PM photocathode. The vertical scale is logarithmic and represents the light intensity in arbitrary units before cell calibration. The curves exhibit the same behaviour. Neglecting the small edge effect far from the PM (right side of the curves), the attenuation length is of the order of 2 m. Crossing muons that release about 33 MeV produce an average number of the order of 100 photoelectrons (spectrum of Fig. 10b).

4.5 Electron Spectra and Energy Resolution

10, 25 and 100 GeV data have been recorded at two high voltage settings. Fig. 11 presents the calibrated 25 GeV spectra obtained within the 3 x 3 central core of the detector installed at CERN (Fig. 6), when the beam hits a 4 x 4 mm^2 area around the axis of the central cell. Two different abscissa scales are used in order to make the energy deposit in external cells

more visible. Both represent the calibrated charge. 80% of the total energy is deposited in the central crystal. Similar results are obtained at other beam energies as it is illustrated on Fig. 12 which displays the normalized central counter spectra at 10, 25 and 100 GeV.

The total energy summed over the 21 calibrated counters of the matrix is shown in Fig. 13 for electrons traversing the central crystal near its axis, in a 6 x 6 mm^2 area.

The shape of the spectrum is nearly gaussian except for a small tail at the left side. The resolution has been determined by fitting the spectrum with a gaussian between 50% of the maximum on the left wing and 10% of the maximum on the right wing of the peak.

The result of the fit includes the beam momentum spread $\sigma p/p = 0.4\%$ and an electronic noise component which can be split in two contributions : the first one is correlated to pedestal fluctuations; the second is due to the minimum detection threshold of 3 in ADC units which increases the fluctuation of the number of unrecorded small amplitudes. The corrected resolution is presented in Fig. 14 with error bars. The prototype matrix resolution is better than 1% above 25 GeV. It is fitted by the following relation :

$$\frac{\sigma E}{E} = \frac{3.25 \pm 0.6}{\sqrt{E}} \oplus 0.8 \pm 0.06 \qquad (1)$$

Both errors are statistical*. These results are in agreement with a preliminary ones [9] that was quoted without errors bars. The difference between the present constant term value and the one quoted in [9] reflects the systematic uncertainty due to experimental conditions of the test.

Pure photoelectron statistics should contribute to the energy dependent term as $1.7\%/\sqrt{E}$ only, if one extrapolates from muons results (§ 4.4). The residual contribution comes from the structure of multi-cell calorimeters [15].

4.6 Photodiode Tests

A single 24 X_0 crystal (2 x 2 cm^2) has been tested with a photodiode (Hamamatsu S3204-03, 300 μm, 1 x 1 cm^2 area, fully depleted by a -60 volt bias). The signal was fed to a charge preamplifier designed for L3 experiment by Oakridge Laboratory, followed by a negative output shaping amplifier designed by the Electronic Department of IPN Lyon. Both

---

* The symbol ⊕ implies the square root of the quadratic sum of the two terms.

have a 2 μs shaping time. The shaping amplifier was connected to a Lecroy 2259 peak sensitive ADC.

Fig. 15 shows the spectra of 25 GeV (a) and 100 GeV/c (b) electrons hitting the crystal in a 5 x 5 mm^2 area around its axis. The same optical coupling as for the PM test was used with a collection geometrical factor $\varepsilon_g = 0.25$. To keep the measurements in the same ADC range at both energies, a factor 4 amplification has been applied at 25 GeV. Respective resolutions are roughly 2.7 and 2.3%. The leakage of the 100 GeV shower through the diode is clearly observed.

Fig. 16 displays the spectrum of 25 GeV muons crossing the diode itself after blinding scintillation light by insertion of a piece of black paper. An amplification factor of 2 was applied for ease of comparison with the 25 GeV spectrum of Fig. 15a. A mean number of 32 000 electron pairs are produced in a 300 μm silicium diode crossed by a minimum ionising particle. Using the energy scale set by the 25 GeV spectrum (Fig. 15a) and an overall correction factor, that takes into account a geometrical collection efficiency $\varepsilon_g = 0.25$ and the nominal 55% mean quantum efficiency of the diode, one gets a mean photons number of ~ 120 photons/MeV seen by the diode without Fresnel correction (of the order of 4%).

CONCLUSIONS

For the first time, after optimisation of the industrial growing process for the production of large optically homogenous PWO heavy crystals with a good radiation hardness, an electromagnetic calorimeter prototype made of a matrix of 21 cells with a length of at least 20 X_0 has been tested. An energy resolution of $\sigma_{E/E} = 3.25/\sqrt{E} \oplus 0.8$ has been achieved using XP1911 photomultipliers with a light collection efficiency of only 38% and a non optimised optical coupling.

ACKNOWLEDGEMENTS

The authors are grateful to B. Ille from IPN Lyon who has kindly provided the basic electronics and advices for the photodiode tests and to J.P. Vialle for improvements of laboratory tests software. They are indebted to A. Bazan and T. Le Flour who have modified

and adapted the NA12 acquisition system to the needs of these tests.

They also thank the entire team operating the ULYSSE reactor and more particularly G. Dauphin and J. Safieh from INSTN/SENE CEA Saclay. They are grateful to C. Jeanney from CEA/DAPNIA/SED for his valuable help for optical machining and measurements.

Some participants are indebted to J. Schukraft and to the ALICE collaboration for their financial support.

Finally, they would like to thank M. Kobayashi and T. Tsuru from KEK for fruitful discussions and help during part of the tests and K. Takamatsu and J.P. Stroot for their constant interest and active support.

REFERENCES

[1] Heavy scintillators. Proc. of the Crystal 2000 Int. Workshop, Chamonix, France, Ed. F. De Notaristefani, P. Lecoq, M. Schneegans, Frontières, C58 (1993) Gif-sur-Yvette, France.

[2] S.E. Derenzo, W.W. Moses, "Experimental Efforts and Results in Finding New Heavy Scintillators", Ref. 1, page 125.

M. Kobayashi et al., "PWO scintillator at room temperature", Ref. 1 page 375.

[3] V.G. Baryshevsky et al., Nucl. Instr. and Meth. A322 (1992) 231.

[4] V.A. Kachanov et al., "Beam studies of EM calorimeter prototype built of PWO crystals" reported to the IV Int. Conf. on Calorimetry in High Energy. Sept. 15-19, 1993, Isola Elba, Italy.

[5] L.V. Miassoedov et al., "PWO : a heavy, fast and radiation resistant scintillator for EM calorimeter", Ref. 1, page 437.

[6] L. Nagornaya et al., "Fast scintillators based on large heavy tungstate single crystals", Ref. 1, page 367.

[7] S. Anderson et al., Nucl. Instr. and Meth. A332 (1993) 373. See also Ref. 1.

[8] D.F. Anderson et al., Nucl. Instr. and Meth. A290 (1990) 385.

C.L. Woody et al., IEEE, Trans. Nucl. Sci. 40 n°4 (1993) 546.

[9] V.A. Katchanov et al., Preprint LAPP-EXP-93-08, to be published in the Proc. of IEEE

93, Nuclear Science Symposium, Nov. 1993, San Francisco, California.

[10] M.V. Korzhik et al., "Spectroscopy and origin of radiating centers in PWO single crystals", (Submitted to Physica Status Solidi).

[11] R. Chipaux et al., "Behaviour of CeF_3 scintillator in LHC like environment" (DAPNIA-94-01 to appear in Nucl. Instr. and Meth.).

[12] O.V. Buyanov et al., IHEP 93-144.

[13] M. Kobayashi et al., Nucl. Instr. and Meth. A333 (1993) 429.

[14] V.A. Davydov et al., Nucl. Inst.and Meth. 145 (1977) 267.

[15] T.S. Virdee, "Performance and Limitations of Electromagnetic Calorimeters", Proc. of the Second Int. Conf. on Calorimetry in High Energy Physics, Capri, Italy, Ed. Ereditato World Scientific, Singapore, page 3.

FIGURES CAPTIONS

Fig. 1 1-Absorption coefficient K (left scale) and 2-the γ-ray excited (Co^{57}, 122 KeV) luminescence of a reference crystal at T = 300°K (right scale).

Fig. 2 PWO scintillation decay time spectrum under γ ray excitation (Na^{22}), at T = 300°K.

Fig. 3 The amplitude spectra of PWO et BGO scintillators excited by different energy gamma sources. T = 300°K. [^{137}Cs, ^{241}Am] and Am-Be.

Fig. 4 a) PWO recovery of transparency after γ irradiation (transmission through 1 cm) for enriched Pb^{3+} sample.

b) PWO transparency versus γ absorbed dose (through 1 cm) for depleted Pb^{3+} sample. Bottom curve remind the shape of scintillation spectrum.

c) PWO transparency after fast neutron irradiation. (2.4 cm thick sample)

d) variation of PWO absorption coefficient after fast neutron irradiation. Arrows stand at the light emission peak wavelength.

Fig. 5 Test matrix of Cherenkov radiator and PWO at IHEP.

Fig. 6 The 21 PWO crystal matrix at CERN.

Fig. 7 a) Fraction of the collected charge amplitude A/A(400) versus the ADC gate width

measured after 95 m of cable in IHEP tests.

b) Oscilloscope traces of 100 GeV electrons after 4m of 50 Ω cable at CERN.

Fig. 8 a) The horizontal x position of the center of gravity of the calorimeter signals versus the beam coordinate.

b) Position resolution σ_x versus the beam coordinate x(beam).

Fig. 9 a) The 26 GeV electron shower profile A_6/A_{tot}.

b) Comparison of profiles for different types of calorimeters (see the text).

Fig. 10 a) The signals of muons arriving perpendicularly to the axis of three crystals versus the impact x distance from the photocathode.

b) A typical muon spectrum.

Fig. 11 Typical electron calibrated charge spectra of the 3 x 3 core matrix (CERN) at 25 GeV.

Fig. 12 Spectra of 10, 25 and 100 GeV electrons in the central cell versus the deposited energy.

Fig. 13 Energy spectra of 10, 25 and 100 GeV electrons as measured by the whole prototype (21 cells).

Fig. 14 The energy resolution with error bars after corrections. Dashed curve is the fit by formula 1.

Fig. 15 Electron Spectrum in one crystal viewed by a photodiode at a) 25 GeV with an amplification factor 4 and b) 100 GeV.

Fig. 16 Muons spectrum through the photodiode itself.

Table 1 : Basic characteristics of some heavy crystals

Crystal	Density (g/cm^3)	Radiation length (cm)	Moliere radius (cm)	Light yield (% of BGO)	Decay time (ns)	Peak emission (nm)	Refractive index
BGO	7.13	1.12	2.25	100	300	480	2.15
CeF_3	6.16	1.68	2.63	45	5/20	300/340	1.62
BaF_2	4.89	2.05	4.4	40/160	0.6/630	210/320	1.49
PWO	8.28	0.87	2.19	5	2.1/7.5/26	480	2.16
$NaBi(WO_4)_2$	7.57	0.98	2.66	Č	-	-	2.05
$Gd_3Ga_5O_{12}$	7.02	1.45	2.4	Č	-	-	2.0
PbF_2	7.56	0.95	2.2	Č	-	-	1.82

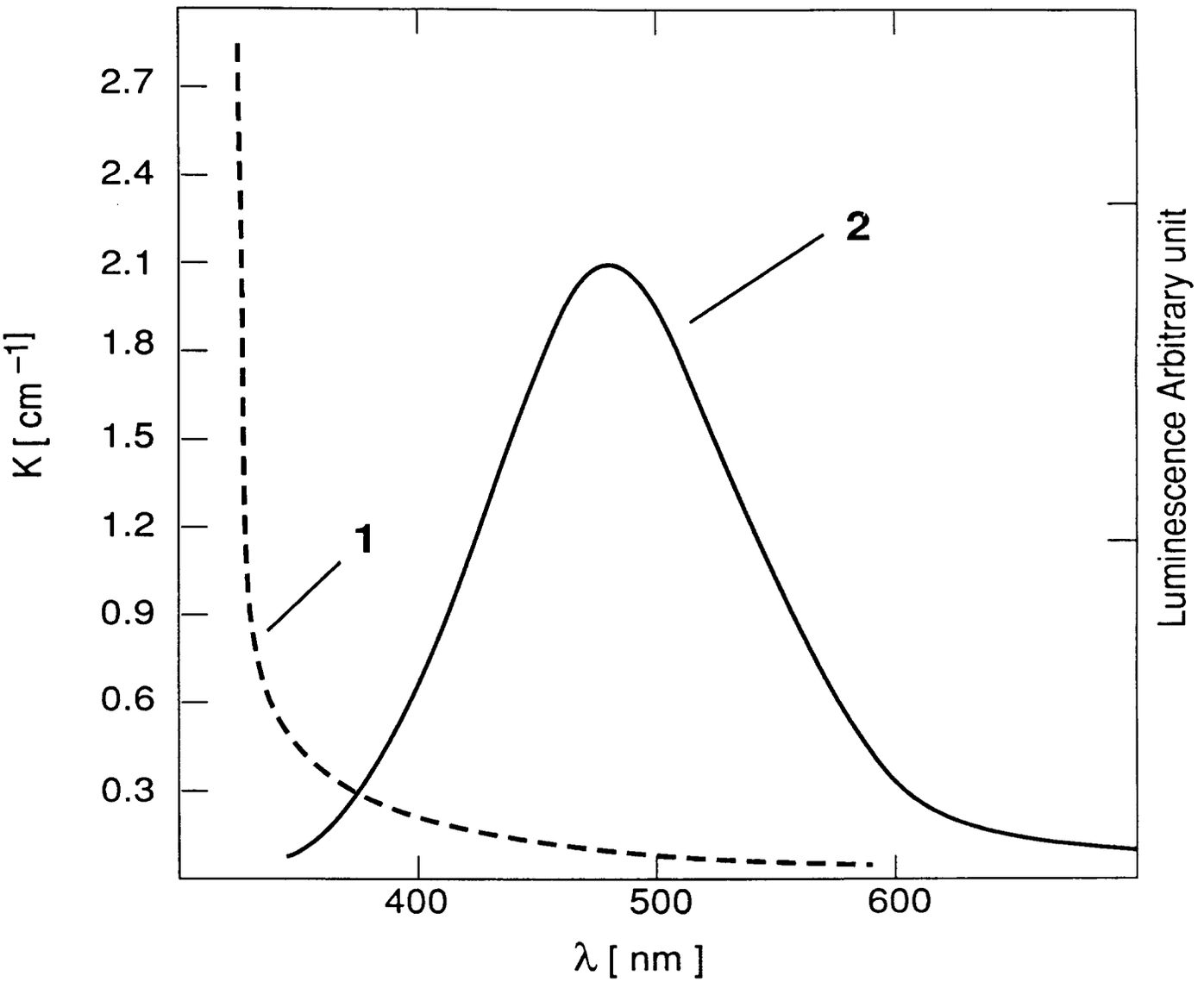
2.7
2.4
2.1
1.8
1.5
1.2
0.9
0.6
0.3
K [cm⁻¹]
1
2
400
500
600
λ [nm]
Luminescence Arbitrary unit

Fig. 1

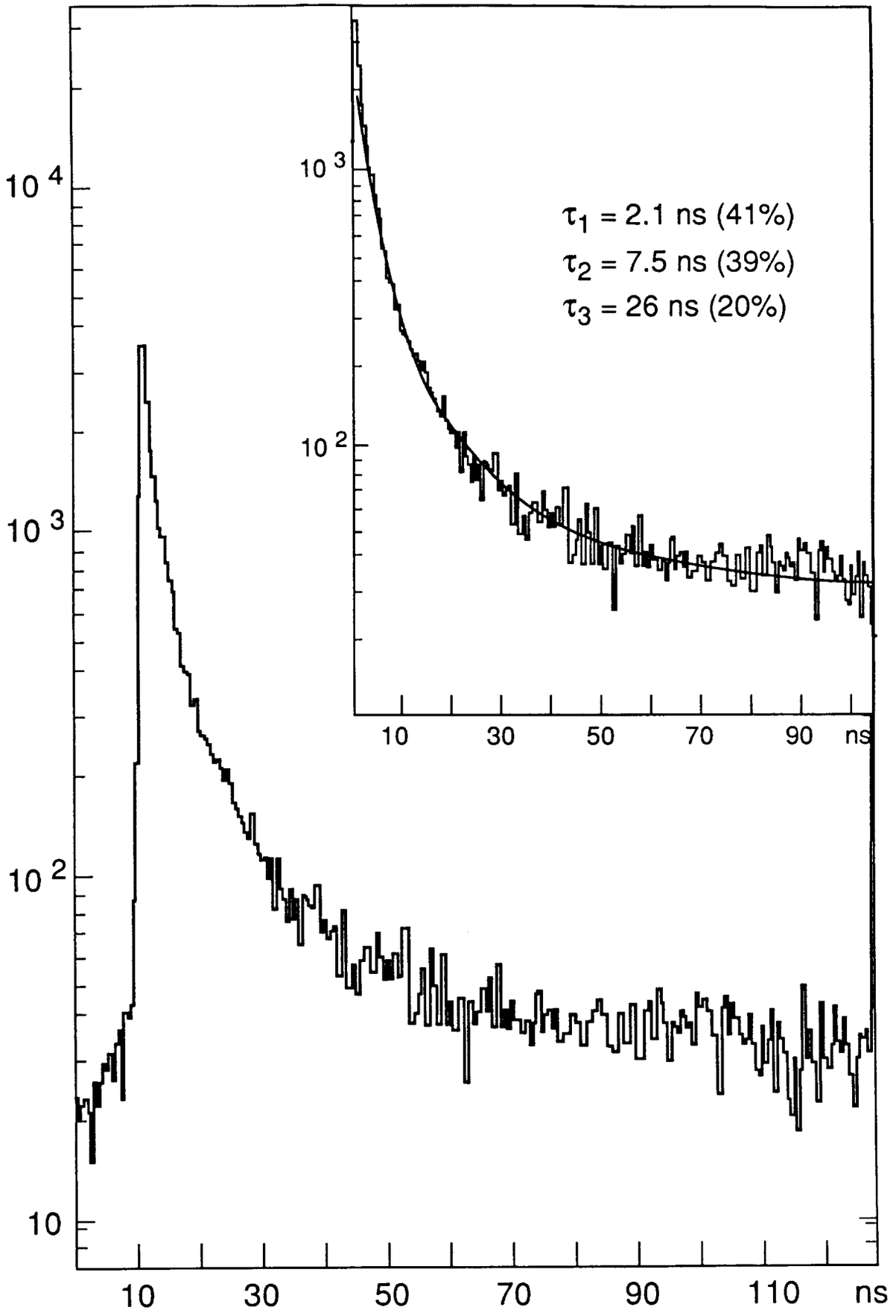
10^4
10^3
10^2
10
10
30
50
70
90
110
ns
10^3
10^2
τ_1 = 2.1 ns (41%)
τ_2 = 7.5 ns (39%)
τ_3 = 26 ns (20%)
10
30
50
70
90
ns

Fig. 2

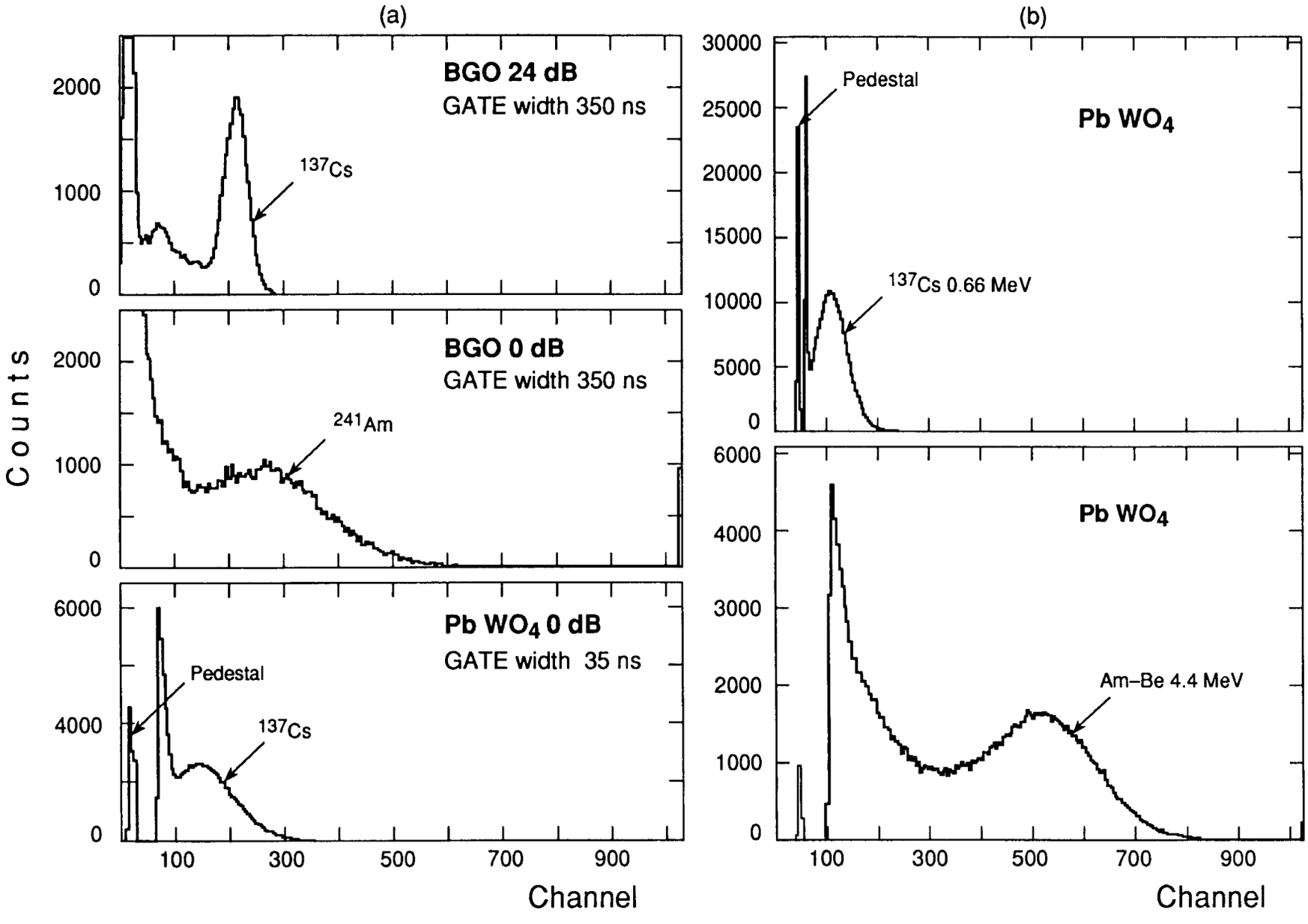
(a)
(b)
BGO 24 dB
GATE width 350 ns
137Cs
BGO 0 dB
GATE width 350 ns
241Am
Pb WO4 0 dB
GATE width 35 ns
Pedestal
137Cs
Pb WO4
Pedestal
137Cs 0.66 MeV
Pb WO4
Am–Be 4.4 MeV
Counts
Channel
Channel

Fig. 3

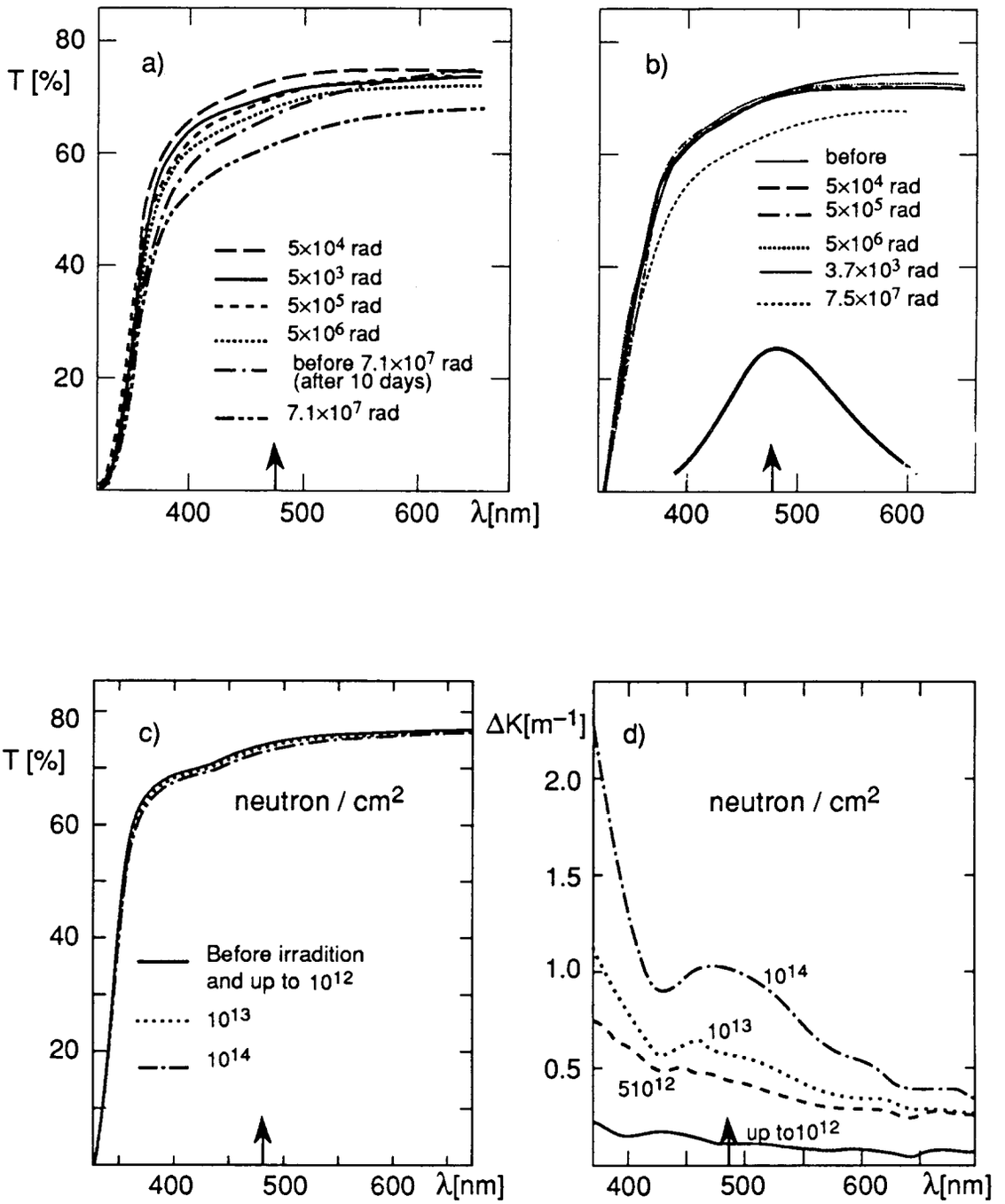
a)
T [%]
80
60
40
20
400
500
600
λ[nm]
5×10⁴ rad
5×10³ rad
5×10⁵ rad
5×10⁶ rad
before 7.1×10⁷ rad (after 10 days)
7.1×10⁷ rad
b)
before
5×10⁴ rad
5×10⁵ rad
5×10⁶ rad
3.7×10³ rad
7.5×10⁷ rad
c)
neutron / cm²
Before irradition and up to 10¹²
10¹³
10¹⁴
d)
ΔK[m⁻¹]
2.0
1.5
1.0
0.5
10¹⁴
10¹³
510¹²
up to10¹²

Fig. 4

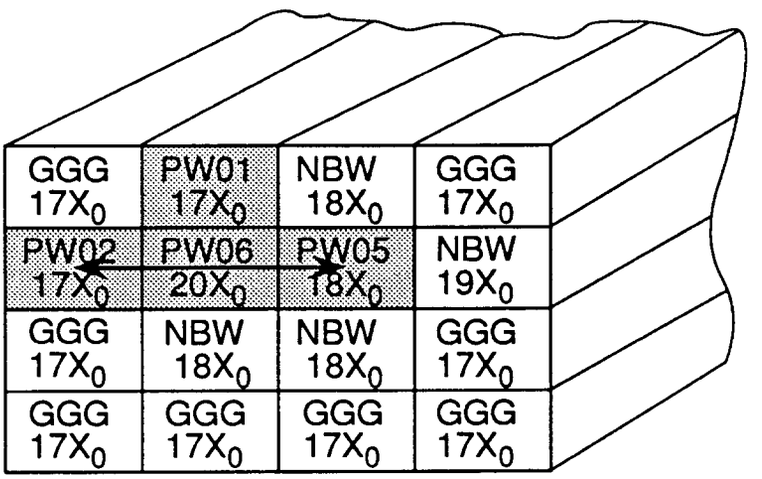
GGG
17X0
PW01
17X0
NBW
18X0
GGG
17X0
PW02
17X0
PW06
20X0
PW05
18X0
NBW
19X0
GGG
17X0
NBW
18X0
NBW
18X0
GGG
17X0
GGG
17X0
GGG
17X0
GGG
17X0
GGG
17X0

Fig. 5

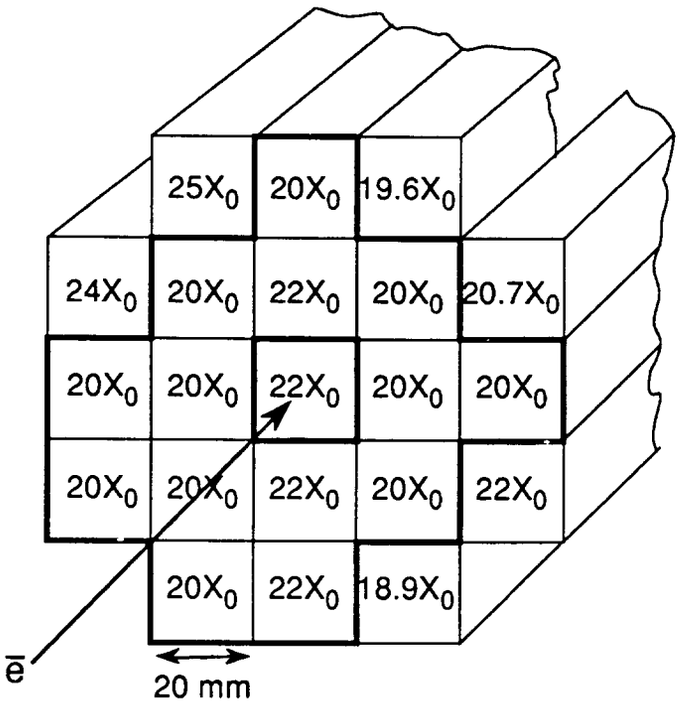
25X0
20X0
19.6X0
24X0
20X0
22X0
20X0
20.7X0
20X0
20X0
22X0
20X0
20X0
20X0
20X0
22X0
20X0
22X0
20X0
22X0
18.9X0
ē
20 mm

Fig. 6

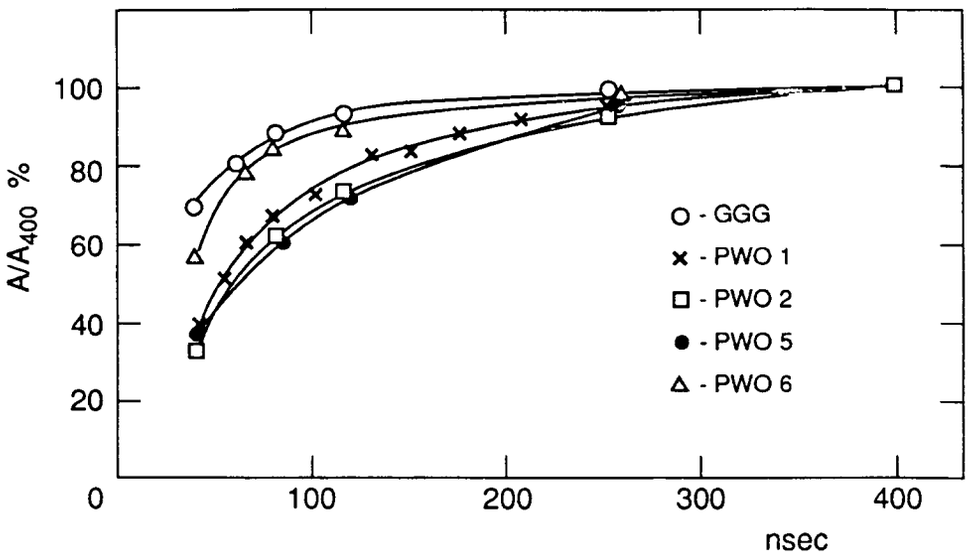
100
80
60
40
20
0
A/A400 %
100
200
300
400
nsec
O - GGG
× - PWO 1
□ - PWO 2
● - PWO 5
△ - PWO 6

Fig. 7a

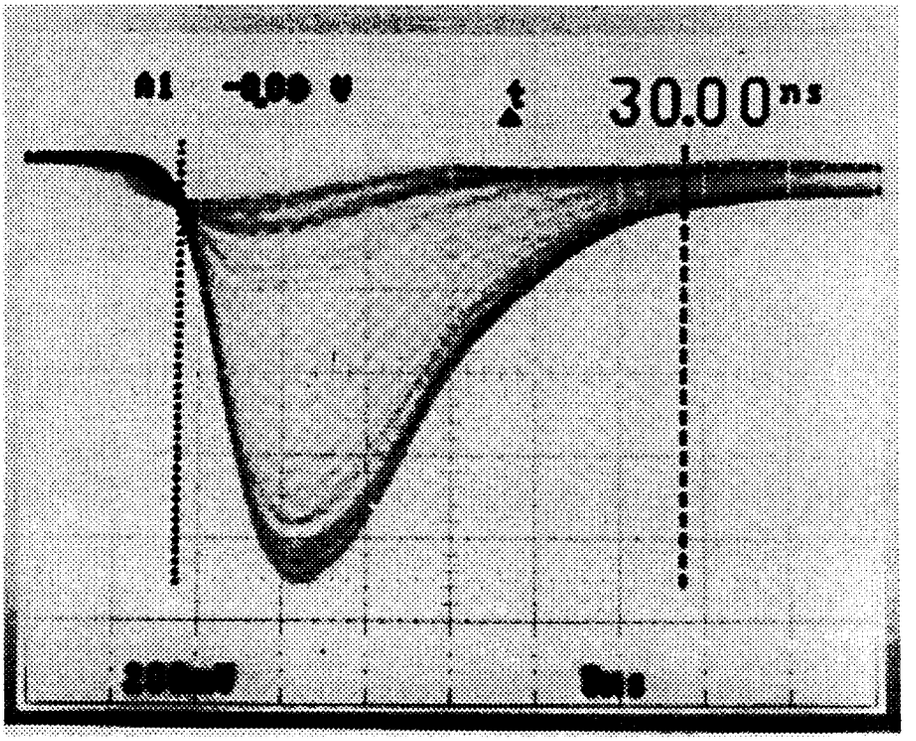
30.00ns

Fig. 7b

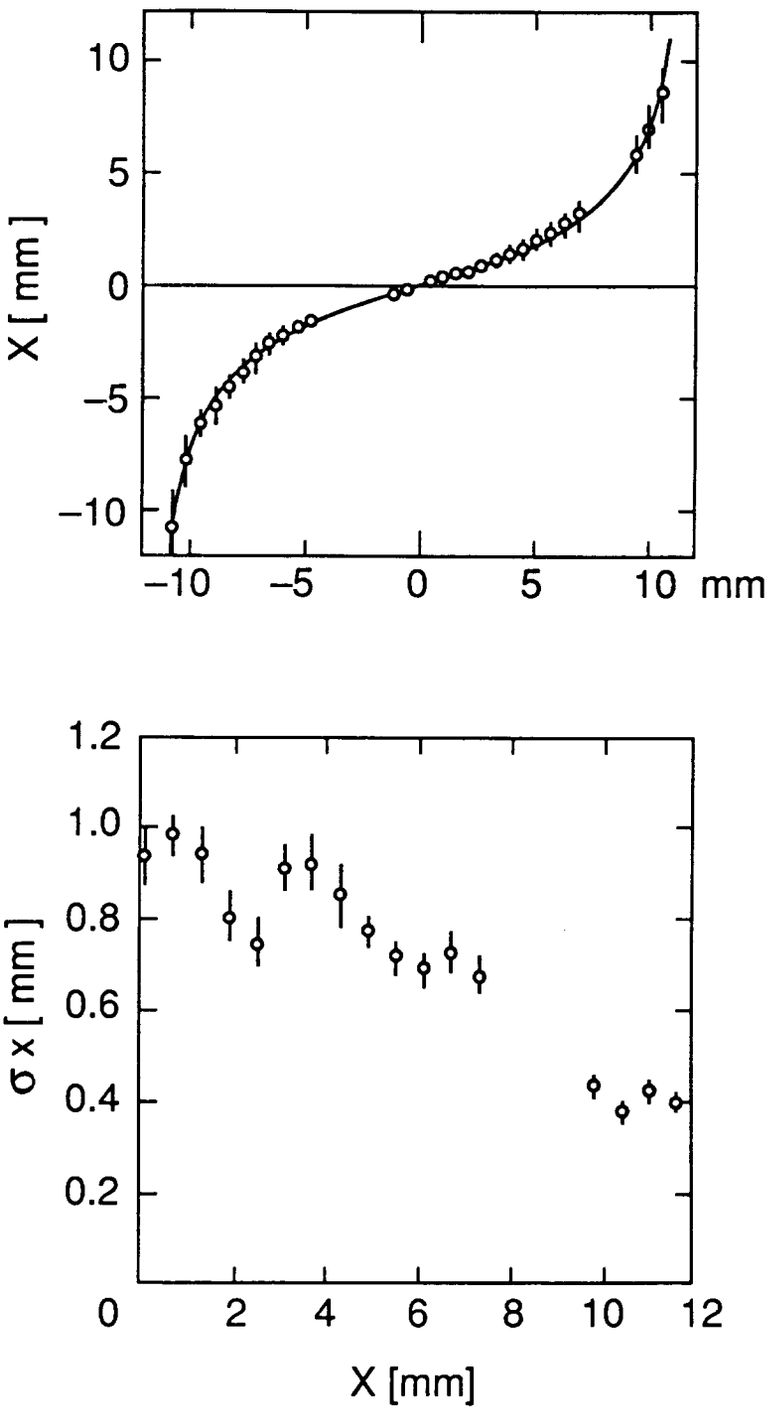

Fig. 8

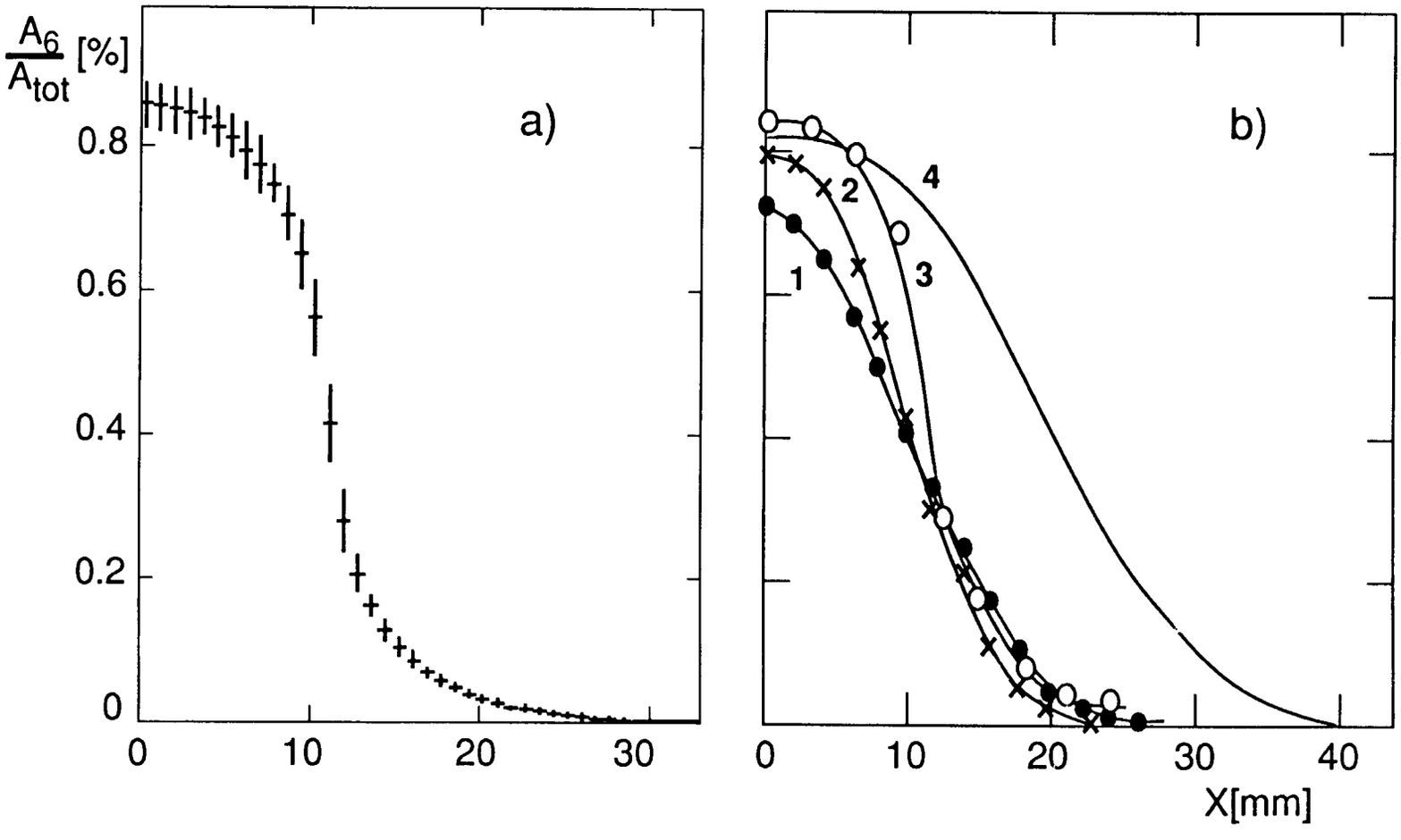

Fig. 9

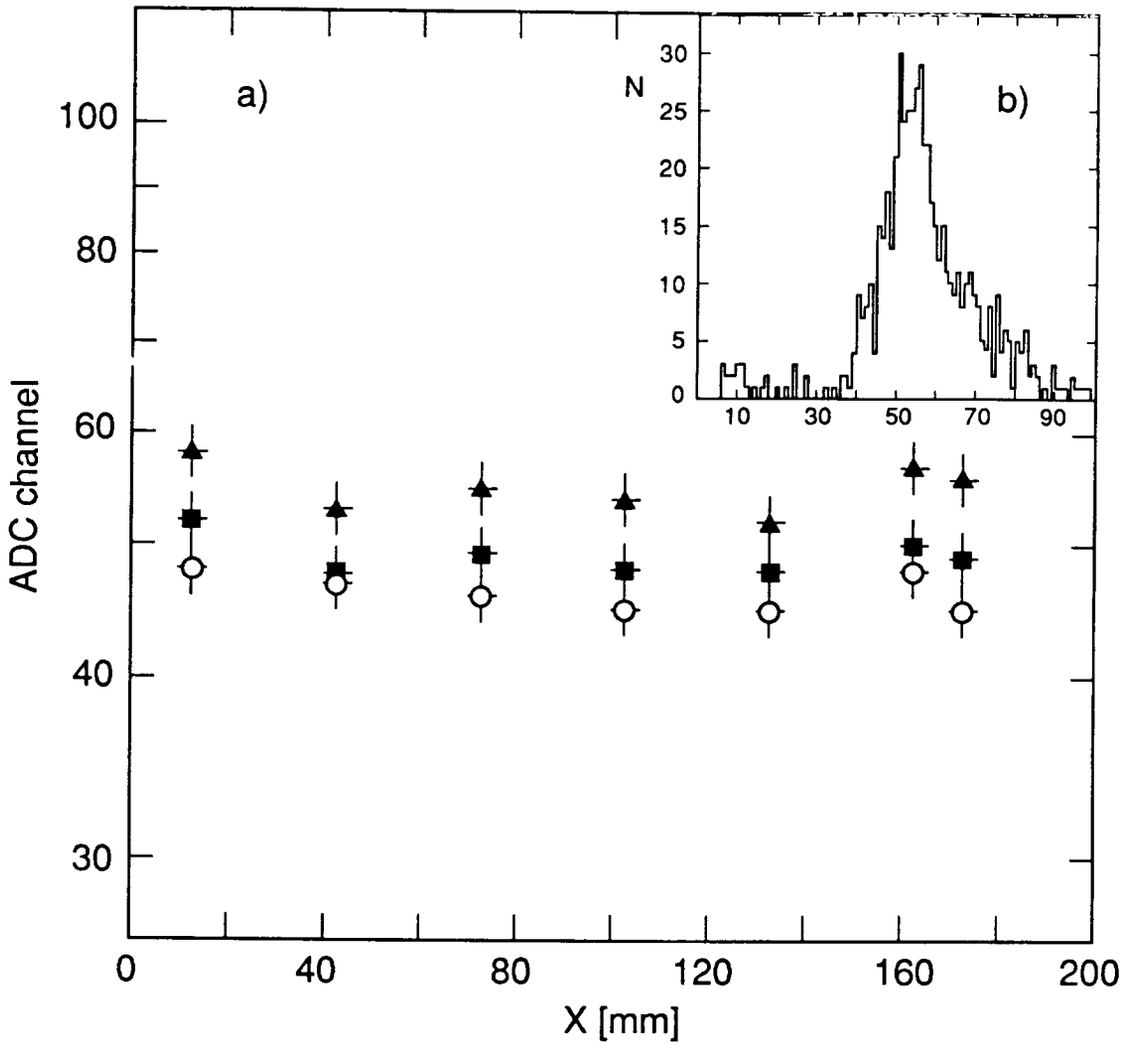
a)
b)
N
ADC channel
X [mm]
100
80
60
40
30
0
40
80
120
160
200
30
25
20
15
10
5
0
10
30
50
70
90

Fig. 10

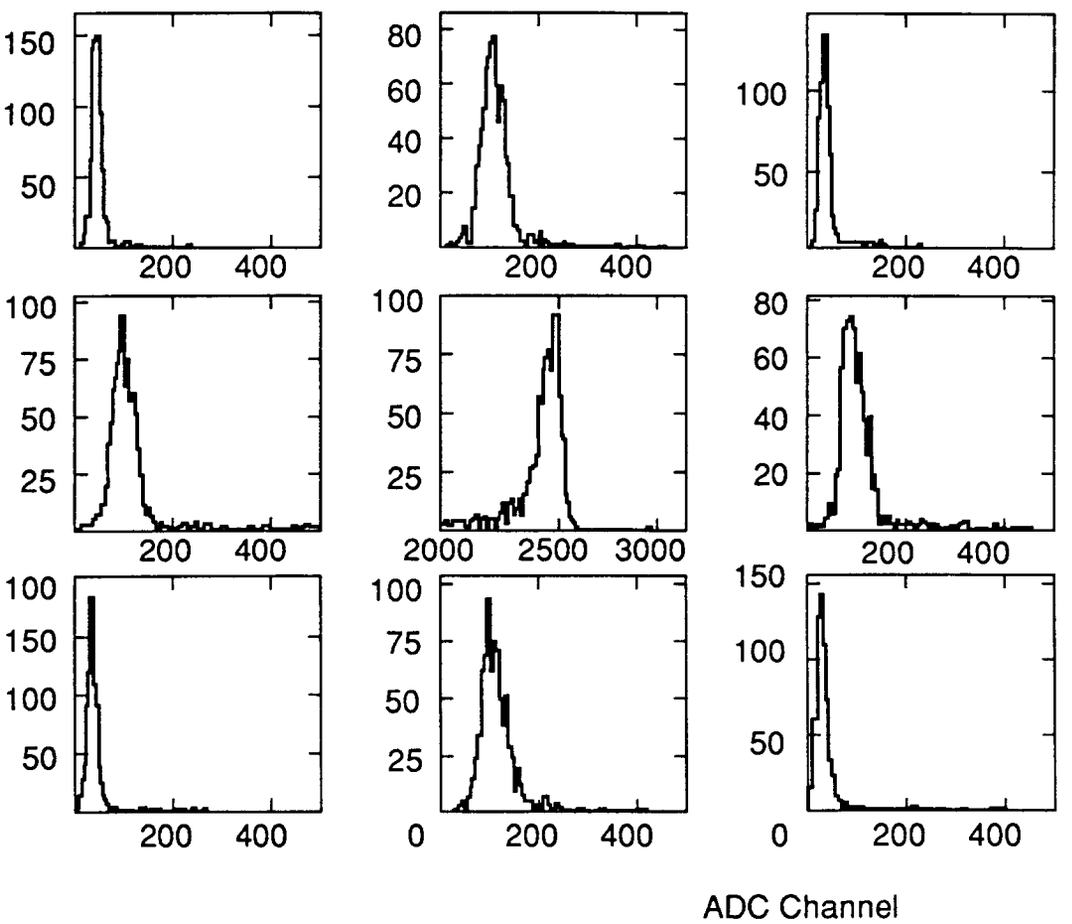
CENTRAL PART of $PbWO_4$ MATRIX
e^- 25 GeV
150
100
50
200
400
80
60
40
20
200
400
100
50
200
400
100
75
50
25
200
400
100
75
50
25
2000
2500
3000
80
60
40
20
200
400
100
150
100
50
200
400
100
75
50
25
0
200
400
150
100
50
0
200
400
ADC Channel

Fig. 11

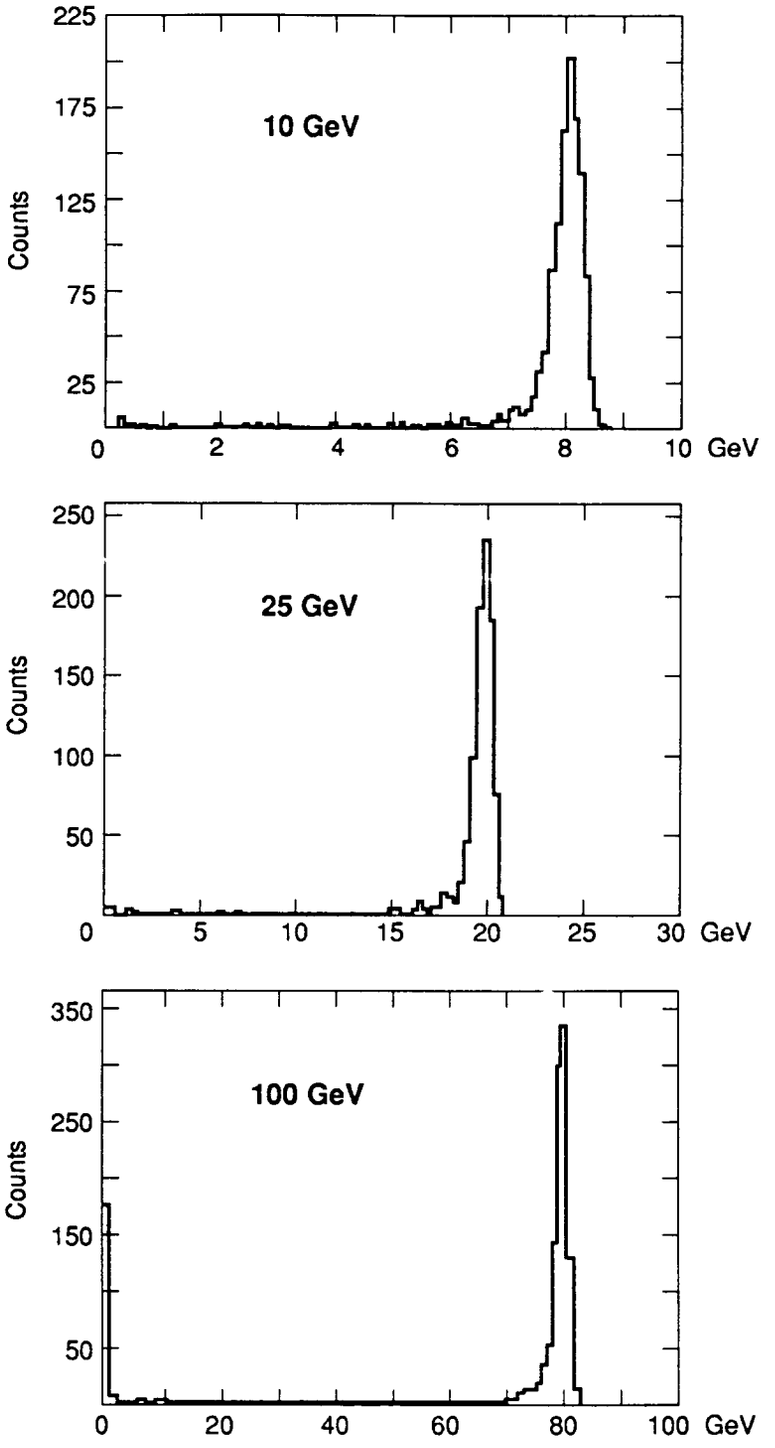
10 GeV
Counts
225
175
125
75
25
0
2
4
6
8
10 GeV
25 GeV
Counts
250
200
150
100
50
0
5
10
15
20
25
30 GeV
100 GeV
Counts
350
250
150
50
0
20
40
60
80
100 GeV

Fig. 12

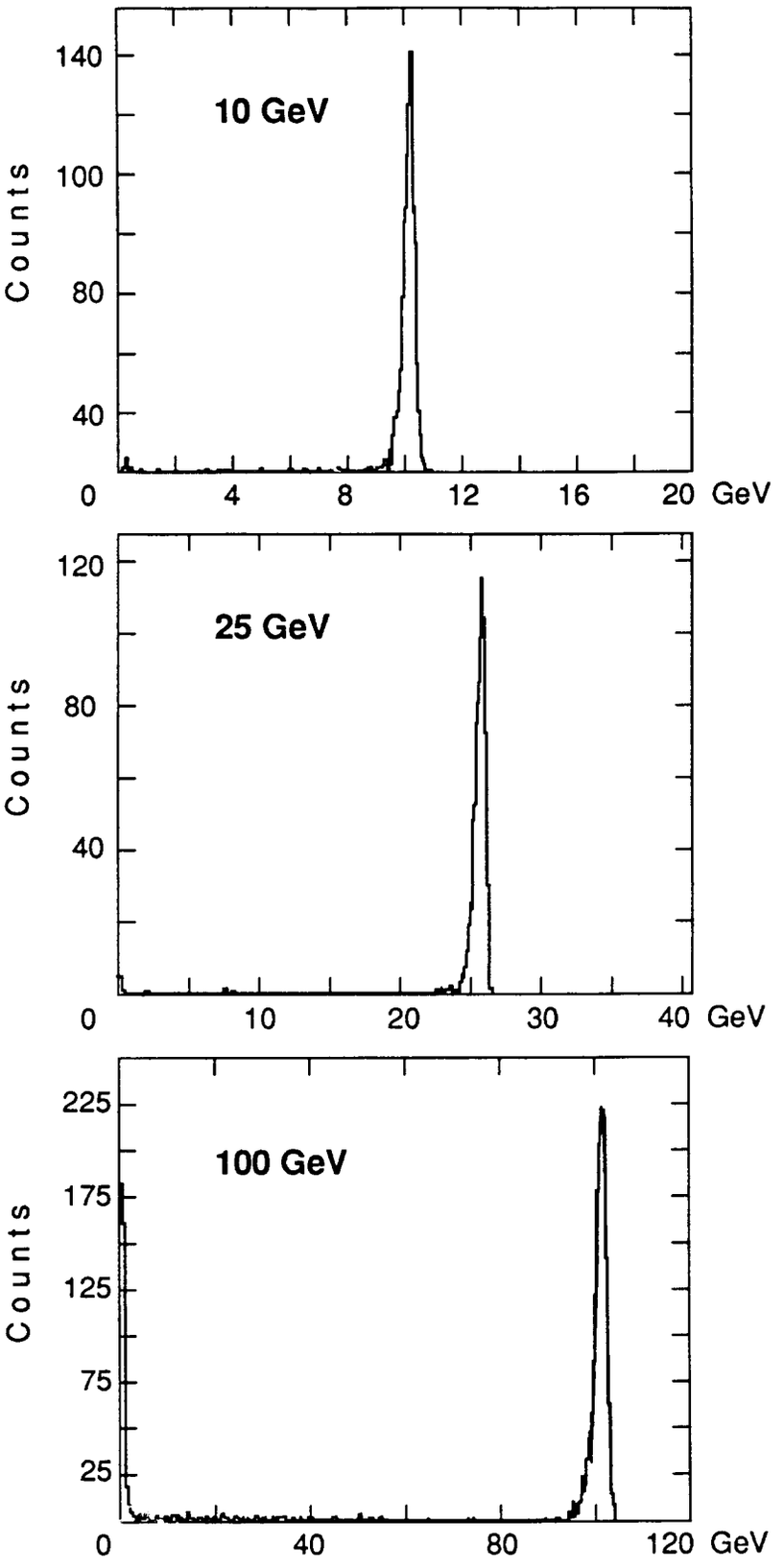
10 GeV
Counts
140
100
80
40
0
4
8
12
16
20
GeV
25 GeV
Counts
120
80
40
0
10
20
30
40
GeV
100 GeV
Counts
225
175
125
75
25
0
40
80
120
GeV

Fig. 13

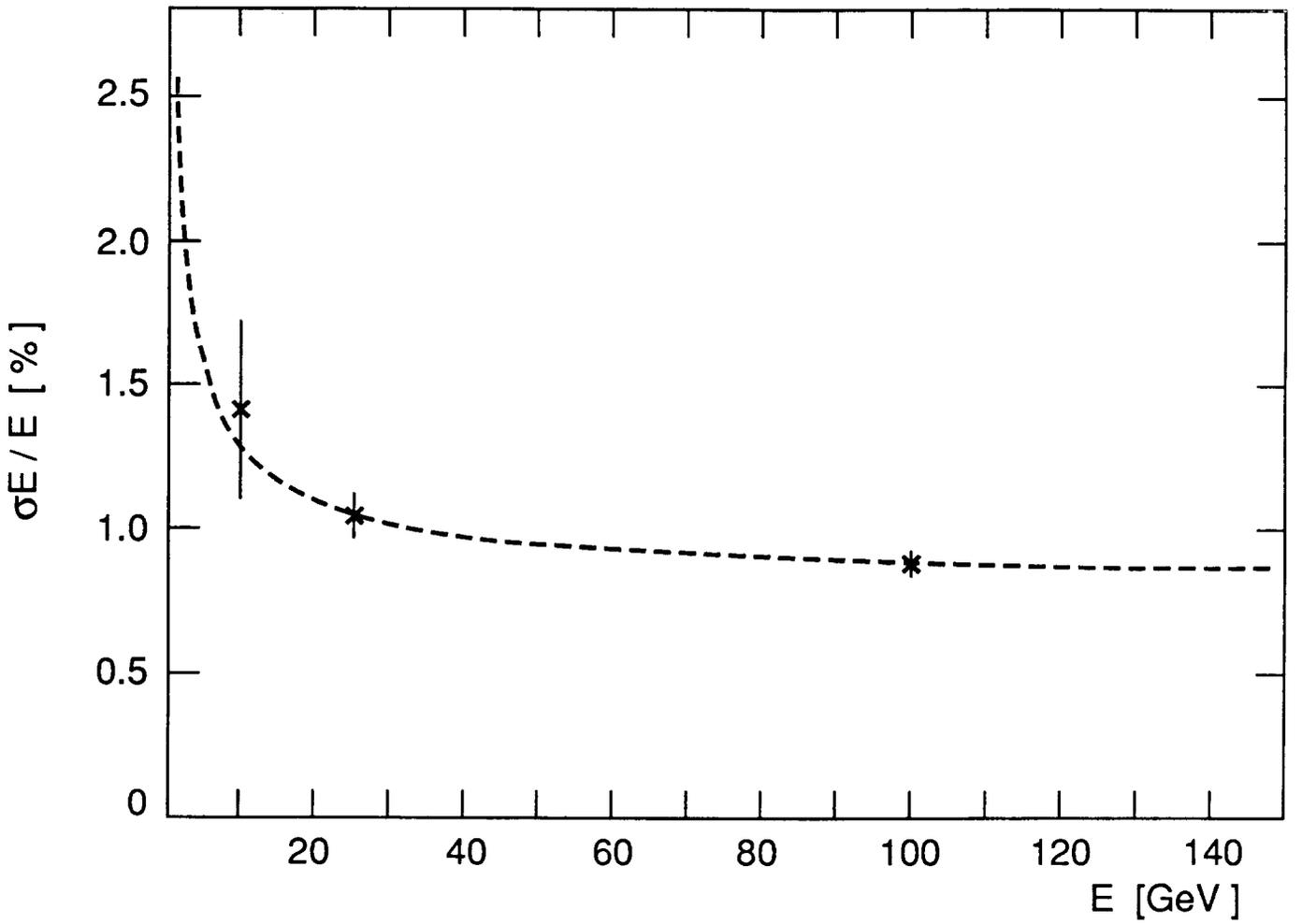

Fig. 14

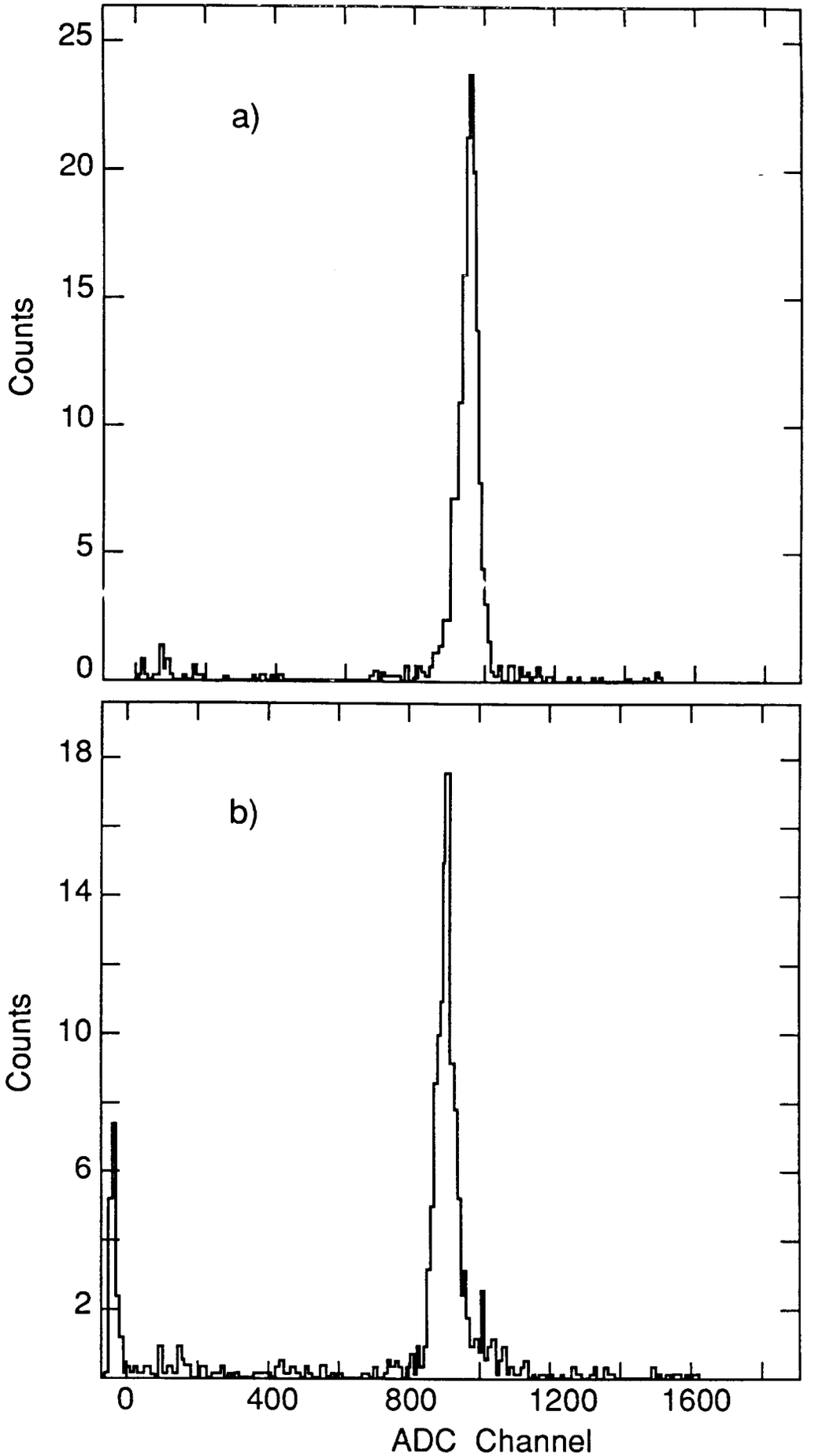
a)
b)
Counts
Counts
25
20
15
10
5
0
18
14
10
6
2
0
400
800
1200
1600
ADC Channel

Fig. 15

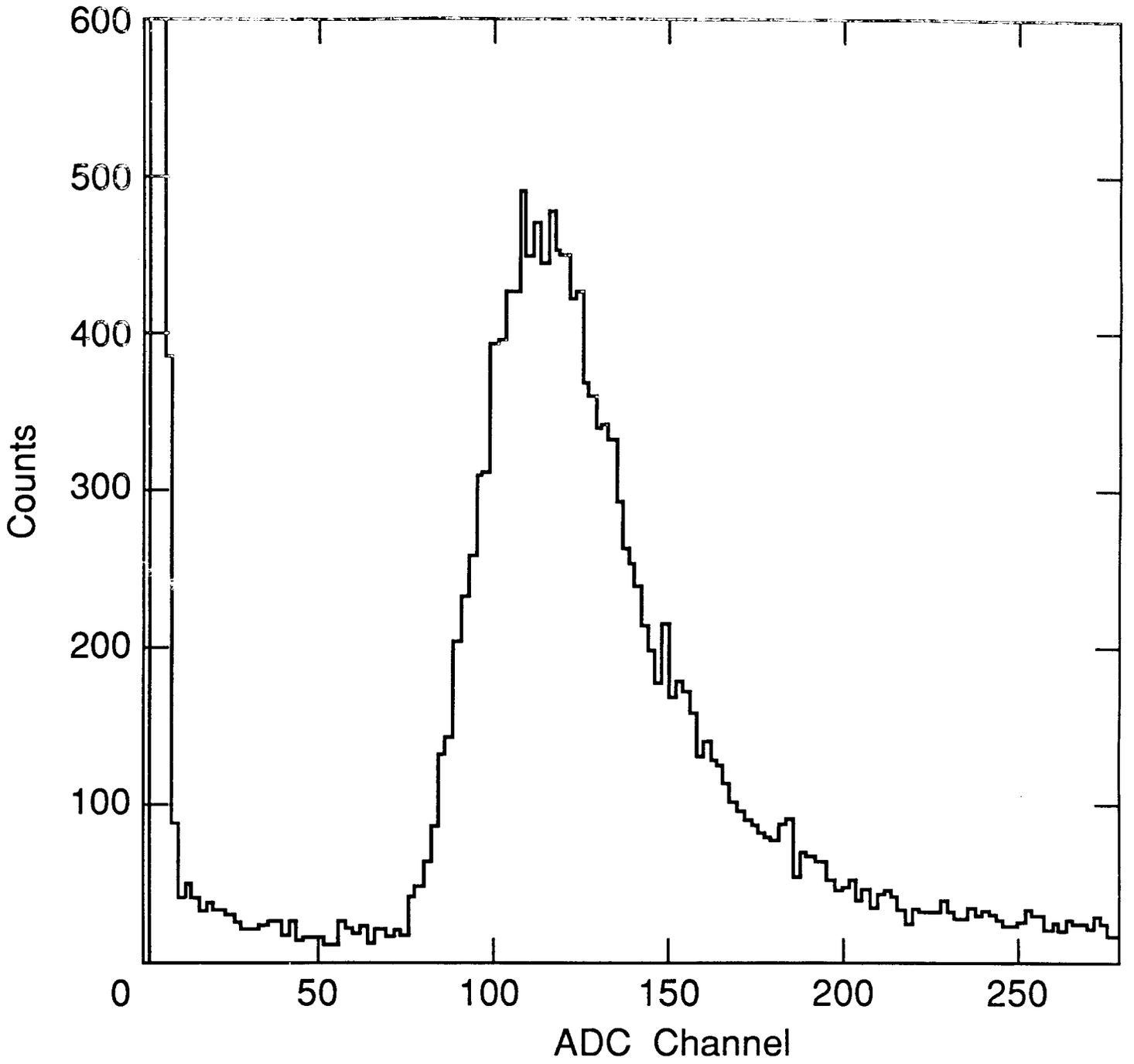

Fig. 16